INTERCALATION OF CIPROFLOXACIN IN SMECTITE: FIRST PRINCIPLES AND MOLECULAR DYNAMICS CALCULATIONS

INTERCALACIÓN DE CIPROFLOXACINA EN ESMECTITAS: CÁLCULOS DE PRIMEROS PRINCIPIOS Y DE DINÁMICA MOLECULAR

A. Lam[a†], G. Rojas-Lorenzo[b], A. M. Ferrari[c], A. Rivera[a], C. M. Zicovich-Wilson[d1] and L. J. Alvarez[e]

a) Zeolite Engineering Laboratory, Institute of Material Science and Technology (IMRE), University of Havana, Havana, CP. 10400. Cuba
b) Instituto Superior de Tecnologías y Ciencias Aplicadas, Universidad de La Habana, Ave. Salvador Allende y Luaces, Quinta de Los Molinos, Plaza, La Habana 10600. Cuba
c) Dipartimento di Chimica, Università di Torino, Via P. Giuria 5, 10125 Torino, Italy
d) Centro de Investigación en Ciencias-IICBA, Universidad Autónoma del Estado de Morelos, Av. Universidad 1001, Col. Chamilpa, 62209 Cuernavaca, Morelos, México
e) Laboratorio de Simulación, Unidad Cuernavaca, Instituto de Matemáticas, Universidad Nacional Autónoma de México, A.P. 273-3 Admon. 3, Cuernavaca, Morelos, 62251, México
† corresponding author

Recibido 16/10/2019; Aceptado 10/5/2020

Two simulation methods, DFT and Molecular Dynamics (MD), have been used to explore the molecular details of the incorporation of ciprofloxacin (cipro) into a clay model. The electrostatic interactions between the compensating cations of the material and the groups with negative charge density of the drug, besides hydrogen bond interactions, are responsible for the stabilization of the cipro in the clay model. The DM results show a rapid migration of some Li^+ cations near the edges, suggesting a charge reorganization process. It is possible to observe at least two attempts of intercalation of the drug. Only when the drug-clay composite material is in contact with water, it is possible to observe the diffusion of a Li^+ cation and the early stages of the swelling process. The results indicate that the cipro molecule in solution plays an important role favoring the stacking process in this clay.

Se han explorado los detalles moleculares de la incorporación de ciprofloxacina (cipro) en un modelo de arcilla, utilizando dos métodos de simulación: Teoría de los Funcionales de la Densidad (DFT) y Dinámica Molecular (DM). Las interacciones electrostáticas entre los cationes del material y los grupos con densidad de carga negativa del fármaco, junto a las interacciones por puente de hidrógeno, son las responsables de la estabilización del fármaco en la arcilla. Los resultados de DM muestran una rápida migración de algunos cationes Li^+ cerca de los bordes del modelo, sugiriendo un proceso de reorganización de carga. Es posible observar al menos dos intentos de intercalación del fármaco. Solo cuando el material compuesto fármaco-arcilla se pone en contacto con agua, se observa la difusión de un catión Li^+ y los primeros estadíos del proceso de hinchazón. Los resultados indican que la molécula de cipro en solución juega un importante papel favoreciendo el proceso de apilamiento en esta arcilla.

PACS: Molecular dynamics methods (métodos de dinámica molecular), 47.11.Mn ; Ab initio calculations of adsorbate structure and reactions (cálculos Ab initio de reacciones y estructura de adsorbatos), 68.43.Bc; porous materials (materiales porosos), 78.55.Mb

I. INTRODUCTION

Clay minerals have been used in a wide range of applications thanks to their chemical and physical properties, which are strongly connected to their structure. From the pharmaceutical point of view, clays and clay minerals have been used as excipients and/or active principles. The high superficial area and the interlayer spaces allow to host drugs, opening the possibility to employ these materials as drug delivery systems [1].

Fluorohectorite belongs to the smectite group of clays. They are 2:1 phyllosilicates that possess a negative net charge. Counter-ions are located between clay lamellar sheets to balance that charge. The swelling property of these clays allows modifications with organic species, yielding materials with potential applications [2–8]. The chemical formula of the synthetic fluorohectorite clay is $M_x(Mg_{6-x}Li + x)F_4Si8O_{20}$, where M denotes either Li or some other monovalent cations. In this silicate, the fraction of M^{2+} ions are substituted by Li^+ in trioctahedral sites, resulting in a structural negative charge of 1.2 e^- per unit cell [9]. Toxicological studies revealed the safety of Li-Fluorohectorite (*LiFh*) when it is administrated orally to experimentation animals [8, 10]. On the other hand, Ciprofloxacin (1-cyclopropyl-6-fluoro-4-oxo-7-(l-piperazinyl)-1,4dihydro-quinoline-3-carboxylic acid) is one the most widely used antibiotics, with high antibacterial activity that is orally administrated to patients in its hydrochloride salt form. The incorporation of ciprofloxacin (cipro) into the interlayer space of a *LiFh* can be found in the literature [5, 10]. Those studies indicated that *LiFh* is active with temperature. This fact could lead to design a temperature-controlled drug delivery system.

The use of experimental techniques to understand details related to the incorporation and adsorption of organic species, as well as the groups involved, cannot provide full details of the processes, so the use of computational techniques could be a very useful alternative for this purpose [11, 12]. Theoretical reports of host-guest interactions in clays have been mainly

conducted taking into account that guest molecules are already inside the interlayer spaces. Only few simulations about the incorporation processes of molecules inside clays using atomistic simulations have been reported due to the number of particles and the simulation time involved [13,14]. In some cases, mesoscale methods have been used to model these complex processes [12,14]. However, these methods can miss the details of the processes at the nanometric scale.

In this work, different theoretical methods have been combined to get insight into the cipro intercalation process on *LiFh* . First principle calculations were performed to elucidate the *LiFh* -cipro interactions inside the interlayer. The quantum optimized clay-water framework was the starting geometry to create a *LiFh* model that was put in contact with a drug solution. And three different scenarios of clay-drug interactions were studied through Molecular Dynamics simulations.

II. METHODOLOGY

II.1. Periodic quantum calculations

The Lithium Fluorohectorite used in the present simulation was built from the Cambridge Data Base Structure of organic pillared fluorohectorite reported by Breu et al [15]. Different transformations were performed on the unit cell of this starting structure to obtain the $Li-Fh$ model, which represents the clay used in a previous work where the charge per cell is around 1.2 e^- [5]. Firstly, the organic intercalated molecule was removed from the structure. After that, the clay octahedral sheet was arranged in such a way that 2 M^{2+} were replaced by 2 Li^+, creating a framework with charge -2 e per unit cell that was compensated with two Li^+ cations, obtaining the chemical formula $Li_2(Mg_4Li_2Si_8O_{20}F_4)$ per unit cell. These Li^+ compensating cations are located in the interlayer region, close to the tetrahedral oxygens that coordinate the new octahedral *Li*. In order to reproduce the interlayer space obtained in the X-ray powder diffraction pattern of the *LiFh*-cipro composite [5], the c crystallographic parameter was increased to 18 Å. Within such space, it is possible to arrange one cipro molecule -which was put in its zwitterionic form- or twelve water molecules based in the experimental results [16]. These structures were labeled as *LiFh*-cipro and $LiFh - 12H_2O$, respectively. They were optimized using periodic quantum calculations implemented in CRYSTAL14 code [17] as it will be explained below. The starting zwitterionic form of cipro, see figure SI1 in Supporting Information, was also obtained from the Cambridge Data Base [18].

Electronic structure calculations were performed employing the PBE0 approach [19]. The considered basis set was a valence double-ξ with polarization (VDZP) one. The same computational conditions have already been validated in previous works when studying zeolite hydrated models [20–22]. The Hamiltonian matrix has been diagonalized in a set of k-points in reciprocal space generated according to the Monkhorst-Pack prescription [23] with shrinking factor of 2 for sampling the first Brillouin Zone. This gives rise to 8 k-points as all models considered exhibit P1 space symmetry. The tolerances considered in the computation of mono and bi-electronic integrals for the coulombic and exchange series were those recommended in the code manual: 8, 8, 8, 8, 16 [24]. The exchange-correlation contribution has been numerically integrated employing a pruned grid with 75 points in the radial and a maximum of 434 points in the angular parts around the nuclei (see keyword LGRID in the code manual) [24]. The condition for convergence of the SCF part was that the energy difference between two subsequent cycles must be less than $1x10^{-7}$ Hartree.

Geometry optimizations were performed with analytic gradients for both atomic positions and lattice parameters, and a pseudo-Newton algorithm (BFGS) for Hessian matrix update [24]. Convergence was tested by considering the default thresholds recommended in the code manual [24]. In order to ensure consistency between the final geometry and the approximations considered for the integral evaluation, the FINALRUN option of the code with value 4 has also been adopted [24].

In addition, for the *LiFh*-cipro system, Grimme D2 correction [25] was considered in order to include the dispersion forces contribution. The geometry optimization at PBE0-D2 level will permit a correct evaluation of the interactions present in the system.

II.2. Molecular dynamics simulations

Three different scenarios of clay-drug interactions were studied through Molecular Dynamics simulations: 1) the clay in contact with the drug solution (*LiFh-cipro-out*), 2) the drug inside the clay, at the center of the interlayer, in contact with an external water solution (*LiFh-cipro-in*) and 3) six drug molecules in the interlayer of the *LiFh* clay crystal (*LiFh-6cipro*). In the first system, the first stages of the drug incorporation process into the clay interlayers were modeled. The second system assumed that the drug was incorporated into the interlayer space and host-guest interactions and possible drug desorption process were evaluated. The third system try to get a deeper understanding of the drug-drug interactions inside the clay crystal, assuming that full incorporation of the cipro has been take place.

The simulation cell used in Molecular Dynamics simulation to model the cipro-clay interactions was built in different steps.

The starting clay structure was the *LiFh* unit cell with 12 water molecules ($LiFh - 12H_2O$) previously optimized with the periodic quantum calculation. Water molecules were converted to SPC water keeping oxygen atoms in the position of the CRYSTAL14 optimization and adjusting the hydrogen coordinates in order to reproduce the distance and angles of SPC parameterization [26]. After that, the unit cell model was replicated to generate a $5 \times 4 \times 3$ supercell that contains 720 water molecules in the interlayer spaces. This procedure generated a very homogeneous charge system, not allowing a random charge distribution of the layer sites. This clay model includes three interlayer regions where the drug could diffuse and is enough large to favor this process.

To reproduce the interactions of the clay surface with a solution containing a ciprofloxacin molecule and its possible intercalation, the periodicity in the 010 direction was cleaved. The valences of *Si* and *O* were compensated adding *OH* and H, respectively, ending the tetrahedral clay edges with *OH* groups. Octahedral ions (Mg^{2+}, Li^{+} and F^{-}) were not balanced. It was assumed that they are very well attached by coulombic interactions between them and to the oxygens of the tetrahedral layers. Recently, Pouvreau et al [27] proposed metal $O-H$ potentials terms for clay edge surfaces. Although only Al and Mg were the proposed metals, this strategy should be considered in future simulations involving clay surfaces.

A 30 Å width slab was inserted in the simulation box. The slab region was filled with 1757 water molecules and 1 cipro molecule (mass concentration of 4,66 mg/ml, greater than that experimentally used [5]). These water molecules were randomly located using the watteradd utility of DL_POLY code [28]. Fig. 1 shows the starting geometry of the *LiFh-cipro-out* simulation. The six different interlayer spaces that are in the simulation box (brown rectangle in Figure 1) are labeled as di (i=1 to 6). The cipro molecule is oriented in front of d2 interlayer region.

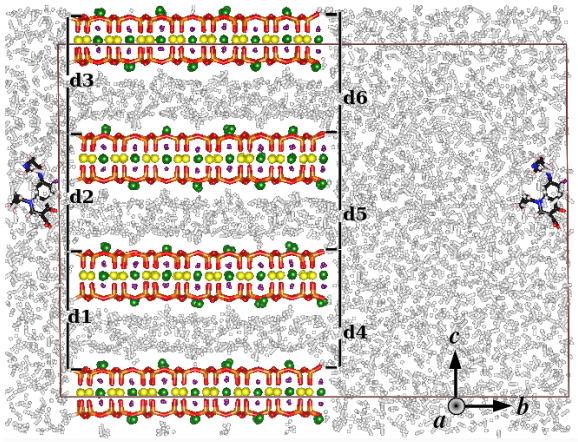

Figure 1. Starting geometry of the *LiFh-cipro-out* MD simulation. The different interlayer distances have been labeled as d1, d2, d3, d4, d5 and d6. Orange, red, green, yellow, violet, black, white, and blue balls correspond to *Si*, *O*, *Li*, *Mg*, *F*, *C*, *H* and *N* atoms, respectively. Water molecules are the white sticks. The simulation box is delimited by the brown rectangle.

All the calculations assume that pH was 7. In the experimental results [5], the cipro solutions (pH near 4.5) were put in contact with the $Li-Fh$ clay during 4h. By the end of the interaction, the pH of the cipro-clay dispersions was around 8, where a true intercalation of the drug at the synthetic clay (277mg ± 10 mg of cipro per gram of clay) was evidenced. In such conditions, an important part of the cipro molecules are in zwitterionic form (i.e., cipro molecules have a positive part related with the protonated amine group and a negative part associated with deprotonated carboxylic group). The *Si* surface edges of *LiFh* should be in the neutral form as $\Xi Si\text{-}OH$ to permit the incorporation of the zwiterionic cipro in the clay. Charged edges, $Si\text{-}O^{-}$ or $Si\text{-}OH_2^{+}$, would have a very strong interaction with the charged groups of the drug, not favoring its intercalation.

On the other hand, *LiFh-cipro-in* simulation box was prepared using the box of the *LiFh-cipro-out*. Twenty six water molecules were replaced at the center of the interlayer by one cipro molecule. These 26 water molecules were added to the solution.

At the same time, *LiFh-6cipro* was built from the DFT calculations of the *LiFh*-cipro system. The unit cell model was replicated to generate a $5 \times 2 \times 1$ supercell. This procedure locates 10 cipro molecules in an interlayer. However, the drug molecules are very close between them that are why we decided to keep only 6 drug molecules in the interlayer, removing 4 drugs from the supercell. In this system periodic boundary conditions in the three directions were applied, simulating the interactions inside the bulk of the crystal. The starting geometries of the *LiFh-cipro-in* and *LiFh-6cipro* MD simulations are presented in Figures SI2 and SI3 of the Supporting Information.

The interactions of the clay atoms were treated with the CLAYFF force field [29] adapted by Marry et al [30]. A small change in the charge of oxygen labeled as O(os) that was set to -1.365 in order to ensure the neutrality of the system and the parameters of Li^{+} were taken from Koneshan et. al. [31]. While water molecules were described with SPC potential [26], the Universal Force Field potential (UFF) was employed to model the cipro molecule [32] and the charges were determined from PBE0/VDZP calculations. Different force fields, like COMPASS [33,34], MM+ [35] and all-atom OPLS have been used to model cipro molecule [36].

UFF is a force field constructed from simple rules and atomic parameters that is capable of reproducing most structural features across the periodic table with errors less than 0.1 Å in bond distances and 5-10° in angle bend. The choice of the UFF resulted from a compromise between good accuracy and availability of force field parameters for all atom types present in the molecular model. Consider the previous experience of using this force field to simulate polypropylene/organoclay nanocomposites [37]. In addition, it was possible to verify that it is adequate to correctly reproduce the cipro geometry in our simulation.

The intermolecular interactions, i.e., the van der Waals and electrostatic interactions, between the atoms of the clay, ciprofloxacin and water molecules, have been treated with the parameters proposed by the different force fields. All details about potentials, parameters and atomic charges used in the simulations are discussed and presented in Tables SI1, SI2, and SI3 of Supporting Information.

Simulations were performed with DL_POLY classical molecular dynamics program [37].

The simulation sequence developed to model the *LiFh-cipro-in* and *LiFh-cipro-out* systems was the following: first, the clay framework was fixed and only the Li^{+} compensating cations, the clay terminal *OH*, the water and cipro molecule were relaxing during 10 ps at 300 K in NVT simulation. After that, a MD simulation relaxing all the atoms during 10 ns in NPT ensemble was carried out, controlling temperature at 300 K during the first 20 ps and fixing pressure at 1 atm. Nosé-Hoover thermostat and barostat were used, each with a 100 fs relaxation time, respectively. In all simulations, periodic

boundary conditions were applied, and the time step was 1 fs.

A strategy of 4 steps was followed for the *LiFh-6cipro* system. First, drug and clay framework were fixed and only Li^+ compensating cations were relaxing during 10 ps at 300K in NVT simulation with the time step equal 1 fs. Step 2 kept the same MD conditions and all the clay was permitted to relax while drug atoms were fixed. In step 3 the whole system clay and drugs is relaxed but it was necessary to reduce the time step to 0.1fs. And finally, in step 4, NPT simulation of 2ns was done, with time step equal to 1fs controlling temperature at 300 K during the first 100 ps. Nosé-Hoover thermostat and barostat were used, each with a 100 fs relaxation time, respectively. Periodic boundary conditions were applied.

Electrostatic interactions of the system were calculated using the Ewald summation method. The cutoff for the Coulomb and Lennard-Jones potentials were set to 10 Å for *LiFh-cipro-in* and *LiFh-cipro-out* systems and for *LiFh-6cipro* system they were set to 8.9 Å. The trajectory of the atoms in the NPT simulations was collected each 1000 steps for dynamics and structural analysis. The six different d-spacings of Figure 1 were determined from the collected trajectory for *LiFh-cipro-in* and *LiFh-cipro-out* systems and the histograms were plotted using the Scott's normal reference rule [38,39].

III. RESULTS AND DISCUSSION

The optimized lattice parameters of the DFT (PBE0/VDZP) and DFT-D2 optimizations (*LiFh* – $12H_2O$ and *LiFh-cipro*) and the three MD simulation systems (*LiFh-cipro-out*, *LiFh-cipro-in* and *LiFh*-6cipro) are documented in Table 1. Also, the previously reported experimental values of the organic pillared fluorohectorite [15], the starting geometry, are presented. Note that cell parameters a, b and γ slightly change compared to the structure reported by Breu et al [15]. There is a good agreement between the cell parameters of the DFT results of the *LiFh*-cipro system, and the Molecular Dynamics of the *LiFh*-6cipro system. Meanwhile the cell parameters of the *LiFh*-cipro-out and *LiFh*-cipro-in systems resemble more the geometry of the *LiFh* – $12H_2O$ obtained by DFT calculations. The largest value of b for the *LiFh*-cipro-in was due to the layer displacement and will be discussed below.

Table 1. LiFh-12H2O, LiFh-cipro, LiFh-*cipro-out*, LiFh-*cipro-in* and LiFh-*6cipro* lattice parameters in comparison with experimental results for the organic pillared fluorohectorite [15].

Cell parameters		*a*	*b*	*c*	α	β	γ
DFT	*LiFh* -12H_2O	5.2648	9.0538	17.308	90.40	77.83	90.46
	LiFh-cipro	5.2728	9.0433	18.189	84.64	98.54	90.11
DFT-D2	*LiFh*-cipro	5.2128	8.9615	17.558	85.23	99.80	90.03
	LiFh-cipro-out	5.8073	9.0501	19.088	90.44	77.83	90.22
MD	*LiFh-cipro-in*	5.8071	11.76	19.087	90.446	77.83	90.227
	LiFh-6cipro	5.6198	9.6385	19.386	84.638	98.54	90.107
Brue et al [15]		5.2635	9.1278	13.984	90.00	96.89	90.00

When the drug is intercalated in the clay model, α is the parameter that changes the most, it decreases almost 6°. Meanwhile, β changes significantly in those systems with water, *LiFh* – $12H_2O$, *LiFh-cipro-out* and *LiFh-cipro-in* (around 19°) leading to a deformation of the clay framework. It is well known that the clay cell parameters could change depending on the clay-guest interactions. The frameworks of these materials are more flexible than other aluminosilicates, like for example zeolites. Specially *c* and β, the first related with the size and number of the molecules host in the interlayers, the second associated with the deformation of the hexagonal cage due to the host-guest chemical interactions. This fact indicates that different guest-host interactions are established in such a way that they produce different reorientations of the clay structure.

III.1. Quantum calculations: Clay-drug interactions

Fig. 2 shows the geometry of *LiFh*-cipro after the PBE0/VDZP optimization. The drug was placed in such way that the carboxylic group was interacting with one of the Li^+ (Li1) and the fluorine of the quinolone ring with the second Li^+ (Li2), both as compensating cations. These are strong electrostatic interactions. From Fig. 2 it is possible to know the distances between atoms: for example, the Li1 cation is located at 1.75 Å from the O1 of the cipro, while the distances to the different oxygen atoms of the clay (O5, O6 and O4) are 2.07 Å, 2.22 Å and 2.39 Å, respectively. It is important to note that the Li-O distance in the lithium oxide is 2.0 Å. These results demonstrate that the interaction established between the Li1 cation and the *O* from carboxylic group of the drug is stronger than that of the ionic bond of the oxide and the ionic interaction with the clay. Li2, the other compensating cation, is strongly interacting with F1 (fluorine of the quinolone ring of the cipro). At the same time, Li2 is keeping the coordination with F2, fluorine of the octahedral sheet of the clay. The Li2-F2 and Li2-F1 distances are 1.95 Å and 2.03 Å, respectively. Li2 also keeps coordinated with the six *O* clay of the hexagonal cage because it is located in the middle of the window; see Figure SI4 in Supporting information which also shows the location of Li1 cation, where it is possible to note that it is placed outside of the hexagonal cage. That is why it is only coordinated with three *O* of the clay.

The stabilization of the drug inside the clay is also associated to the hydrogen bonds involved in the system. These can be classified in three types: the drug-clay H-bonds, the intermolecular drug-drug H-bonds and intramolecular drug H-bonds. Considering the H-bond distances up to 2.6 Å, there are 7 of the first type, 2 of the second and 15 of the third. It is worth noting that an important intermolecular

H-bond was established between the ketone oxygen (O3) and the hydrogen of the amine group H1 (see Fig. 2) at a distance of 1.52 Å. In a previous work a variation in the wavenumber of the band assigned to the C=O ketone, was observed through infrared spectroscopy [5] and was explained based on the drug-clay interaction. Our results suggest a new possible interaction, where the ketone group is involved in an intermolecular hydrogen bond interaction. It indicates that the guest confinement inside the interlayer space of the clay is another important factor to be taken into account.

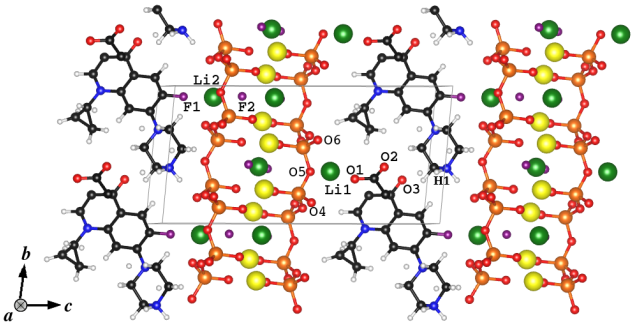

Figure 2. Optimized geometry of the PBE0/VDZP calculations of cipro molecule inside *LiFh* model. The simulation cell is inside the gray rectangle. Orange, red, green, yellow, violet, black, white, and blue balls correspond to *Si*, *O*, *Li*, *Mg*, *F*, *C*, *H* and *N* atoms, respectively.

III.2. The role of dispersion forces

When London type interactions (dispersion) are taking into account in DFT optimization a new final geometry is obtained. The drug is confined in a narrower interlayer space (c decreases by 0.6 Å) favoring the formation of two new clay-cipro H-bonds, while reinforcing a significant number of H-bonds interactions by shortening the *O* clay-H drug distances. This reduction of the d-spacing also decreases the Li^+-O and Li^+-F distances associated with the electrostatic interactions. Energetically, the inclusion of dispersion interactions stabilizes the system in 179 kcal mol^{-1}. This stabilization is not only due to the contribution of the dispersion forces, since in the new scenario there is a significant increase in the contributions of the Coulombic and the H-bond interactions to the total energy of the system. Dispersion interactions play an important role in reproducing the interaction of the host-guest clay interactions and should be take into account in the DFT calculations of these systems.

Table SI4 records the most outstanding distances, hydrogen bonds and the energy values reported by PBE0 and PBE0-D2 calculations.

III.3. Molecular Dynamics Simulations

III.3.1. *LiFh-cipro-out*

A movie with the trajectory of the 10 ns simulation of the interaction between *LiFh* model and ciprofloxacin solution can be found in the video presented in https://www.youtube.com/watch?v=Kic_Fvpl3S4. As can be seen in different moments, the cipro molecule approaches the clay and interacts with the surface. Different kinds of interaction were identified. Fig. 3 shows different moments of the simulation that will be discussed below.

It is important to note that during the first steps of the simulation a rapid migration of Li^+ compensating cation is observed. At the beginning, Li^+ cations moved to the center of the hexagonal cavity, as was observed in Li2 of the quantum calculations (see Figure SI4). A significant migration took place in those Li^+ closest to the surface that define d4, d5 and d6 interlayer distances, see Fig. 1. And was not observed at the other clay side (d1-d3) where M^{2+} octahedral cations were in the edge sites. These Li^+ compensating cations were accommodated in the octahedral sheets between the clay and water molecules of the solution. This fact could indicate a charge reorganization process in the clay framework when it is put in contact with a solution. And it could be the starting point of a possible cation exchange process between Li^+ and the cipro. Two main reasons induced dipole along clay layer b-axis: the border effects and asymmetric cleaving. And these facts, instead of the possible force field limitations, permit the Li^+ interlayer migration.

During the simulation, cipro molecules diffuse in the solution. At 3.3 ns they began to intercalate at the interlayer region, as can be seen in Fig. 3a. This process took place during 0.2 ns until the drug came back to the water solution. It is important to note that the amine group of ciprofloxacin (with q = +1*e*) is the region of the drug that leads the intercalation process. Another short attempt of intercalation took place at 6 ns. As can be seen in Fig. 3b at 3.98 ns, and also in Figure SI5 of Supporting Information, even when the drug does not intercalates, the clay sheets that define d4, increase their separation due to the effect of drug interaction. This phenomenon can be observed for the layers during the simulations, and it should carry to the incorporation of the host molecule.

Also, an interaction between the oxygen atoms of the drug and the surface octahedral cations of the clay takes place at 8 ns, in particular with the Mg^{2+}, and in some cases with the opposite surface that was enriched with Li^+ migrated compensating cations (see Fig. 3c).

Fig. 4 shows the behavior of the d-spacings when the drug solution is put in contact with the clay model during the first 10 ns.

The interlayer spaces are mainly between 18-19 Å. However, d3 and d6 are between 20-21 Å. Note that during all the simulation, three water layers stayed inside the interlayer spaces. And even when the clay model was in contact with a solution with high water content it was not observed any displacement of clay layers that could indicate a swelling process. The short simulated time does not allow for the observation of all processes occurring in drug intercalation. Based on that, it is expected that only first stages of the intercalation could be modeled, and they would be associated with the interaction between the clay surface and the drug.

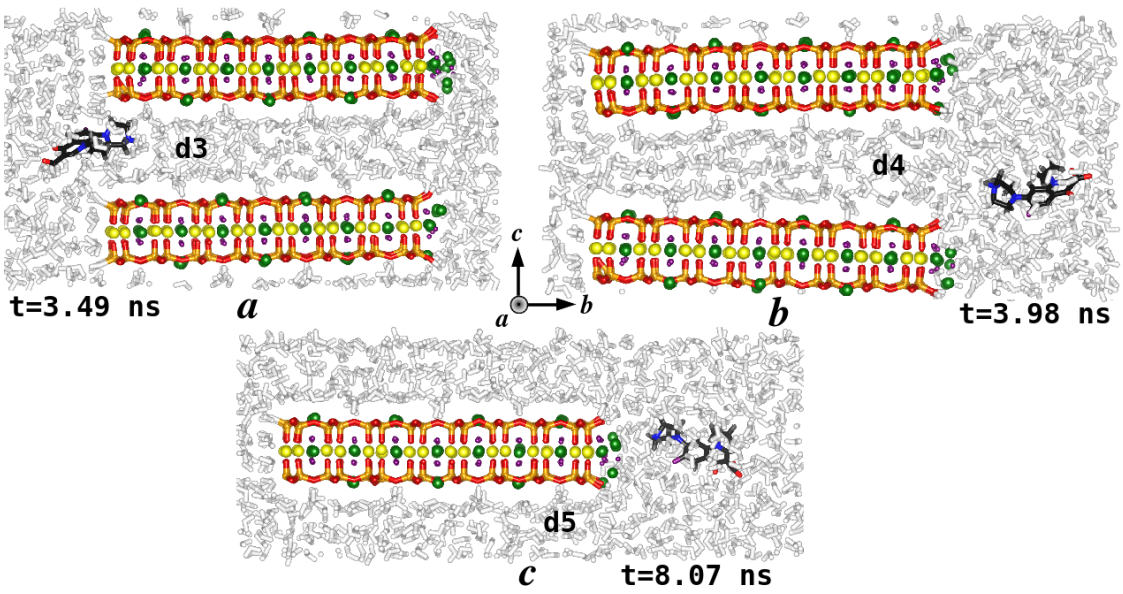

Figure 3. Different snapshots of the MD simulation. Orange, red, green, yellow, violet, black, white, and blue balls correspond to *Si*, *O*, *Li*, *Mg*, *F*, *C*, *H* and *N* atoms, respectively.

III.3.2. *LiFh-cipro-in*

The interaction of the ciprofloxacin hosted in the center of the interlayer of *LiFh* during the first 10ns can be observed in the video presented in https://youtu.be/UjbVv6Z1C4c. Until the 53 ps, the cipro molecule interacted strongly with the clay interlayer, specially, the oxygens of the carboxylic group and the lithium compensating cation (Li^+). Figure SI6 of Supporting Information shows the rdf of Li^+ and the *O* and F of clay and drug and also the rdf H-Oclay. The average distance Li^+-O1 is 2.22 Å, while the Li^+-O2 is 2.67 Å. The charges of these two oxygens are shown in Table SI1. These strong interactions almost anchored the drug to the clay layer, which limits the possibility that it may adopt other configurations. The Li^+-O1 distance only change from 1.99 to 3.27 Å and the Li^+-O2 distance from 2.04 to 4.53 Å. In spite of this fact, during the simulation, the drug molecule tried to change its conformation, favoring that the fluorine atom of the drug can interact with two Li^+ cations of the next layer. From the 117 ps, the average distances between the two Li^+ neighbors to the F are 5.46 Å and 6.77 Å. As can be seen in the movie, during the simulation the drug could adopt other conformations inside the interlayer space favoring other interactions such as the *F*-Li^+, that could approach to distances lower than 5 Å, see rdf in Figure SI6 of Supporting Information.

Also in this system, as in the *LiFh-cipro-out*, a significant migration took place in those Li^+ closest to the edge that define d4, d5 and d6 interlayer distances. However, an important fact that was not previous observed in the *LiFh-cipro-out* system, is the diffusion of one compensating cation through the interlayer space and to/from the outer water. Around the 4.85 ns, a Li^+ compensating cation left its position at the hexagonal cavity of d3, see Figure SI7a in the Supporting Information. In the period between the 4.96 ns and 5.26 ns, it diffused in the outsider solution (Figure SI7b). Then, it returns to the center of the interlayer space and at the 5.38 ns oscillated near its original position for 0.5ns. During the movement of the clay layers that take place after the 7.24 ns, the Li^+ cation was in the center of the interlayer, Figure SI7c. Finally, at 9.53 ns, it anchored into a hexagonal cavity in the middle of the interlayer, and remained there until the end of the simulation (Figure SI7d). A video with the movement of the Li^+ can be consulted in https://youtu.be/2IL3ib4stm8 . In the video, the water molecules were hidden to improve the visualization.

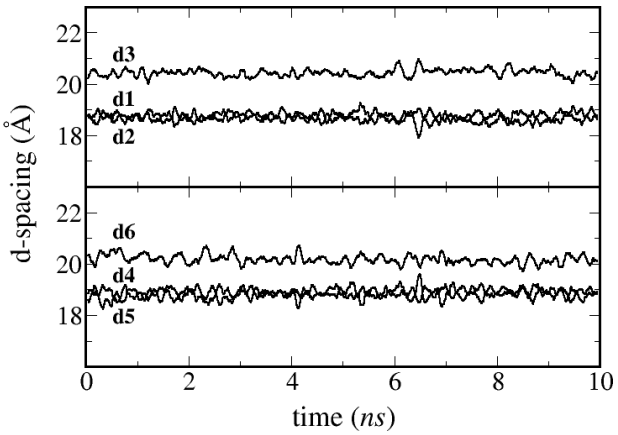

Figure 4. The d-spacings in the *LiFh-cipro-out* system during simulation period.

Other authors have discussed about the mobility of the Li^+ compensating cation. Mignon et al [40] performed a periodic simulation of the hydrated clay, observing that the Li^+ cation remains adsorbed in the surface layer of montmorillonite. This result could justify the fact that most of the Li^+ cations in our simulation were adsorbed in the hexagonal cavity of the tetrahedral layer. On the other hand, Salles et al [41] suggested that during the hydration process in montmorillonite, the small alkali cations (Li^+ or Na^+) could leave the hexagonal site. This motion is favored by the increase in the interlayer distance. In this case, water molecules play an important role modifying the interaction equilibrium between the surface

and the cation and thus induce an increase of the distance cation-surface and allow the cation to reach the interlayer space and be more coordinated by its hydration shell [41]. More recently, Salles et al determined that the Li^+ diffusion coefficient in montmorillonite increases from $5{\times}10^{-25}$ to $1.4{\times}10^{-9}$ m^2s^{-1} with the increase of the amount of adsorbed water in the interlayer [42]. This effect was mainly attributed to both the increase in the interlayer space opening and the high hydration of the compensating cations even at low Relative Humidity (RH). The author proposed that at RH values close to 80 % that correspond to d-spacing around 16 Å, it should be expected that the cations detach from the layer surface and do not interact anymore with it [42]. All the d-spacings during the simulation are bigger than 16 Å.

Up to 7 ns, the high water content of the outer solution had not any effect in the d-spacings of the clay, see Fig. 5. However, from 7.24 ns, different movements produce a displacement of the layers and a noticeable variation of the d-spacing. First, the d4 decreases its size while the d6 opens, allowing an addition of extra water layer (WL). It is possible to note almost 4WL in d6, see Fig. 6a. The d1 also increases its size while the d3 narrows. Then, around 7.33 ns, the system rotates and with this movement the intermediate layer defined by the d1 and d4 only hosted 2WL, note the decrease in the d1 and d4 d-spacing in the small rectangles of Fig. 5 and also the representation in Fig. 6b. After that, a displacement of the layers begins, where d1 and d4 remain constants with 2WL while d2, d3, d5 and d6 increase their sizes, specially d3 and d6, see Fig. 6c. At the end of the simulation the displacement of the layers has decreased, where d1 and d4 decreased their initial value and only host 2WL, while the other interlayers increased their size mainly due to the displacement of the layers, see Fig. 6d. The behavior previously described could indicate a first stage of the swelling process due to the effect of the high-water content of the outer solution.

The histogram obtained from the analysis of d-spacings during the simulations of the *LiFh-cipro-out* and *LiFh-cipro-in* is shown in Fig. 7, and it could be qualitatively compared with the experimental diffraction patterns for the *LiFh*-cipro composite [5]. In that previous work, the 001 reflection (basal reflection) observed with a d-value of 1.7 nm was interpreted as a fingerprint of clay stacks with intercalated cipro, while reflections with d-values equal to 2.1 nm and 2.4 nm were assigned to the possible existence of different conformations of cipro molecules inside the interlayer space or to the presence of water layers in addition to the drug molecule. In our simulation the most intense peak observed for a d-spacing around of 1.9 nm is associated to the clays stacks, with the drug or with three water layers. The peak at approximately 2.0 nm, is associated to the increase of the d-value in d3 and d6 interlayer. Such regions are those that most frequently interact with the drug in *LiFh-cipro-out*, and in some cases could host it. As can be seen, a signal appears with a d-spacing of 1.6 nm in the *LiFh-cipro-in* which is associated to the 2WL of the d1 and d4. For this system the signal is extended until the 3nm due to the effect of the displacements of the layers.

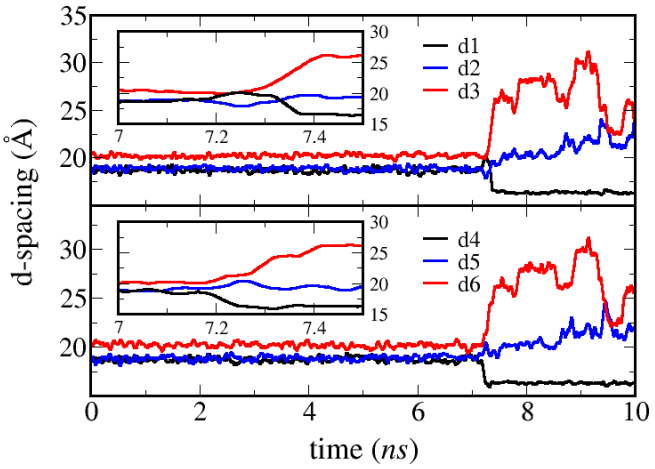

Figure 5. d-spacing in the *LiFh-cipro-in* system during simulation period. In the insets, a zoom is shown into the period between 7 and 7.5 ns.

During all simulation in the *LiFh-cipro-in* system the cipro molecule was in the interlayer of the clay and was not observed any drug desorption process, indicating a strong clay-drug interaction.

III.3.3. *LiFh-6cipro* system

The drug-drug interactions inside the clay can be determined by analyzing the simulation of 6 cipro molecules arranged in the interlayer region of the *LiFh* model used. Fig. 8 shows the radial distribution function (rdf) of the Li^+ with the oxygen atoms of the clay and the oxygens and fluorine atoms of the drug. The results are in good agreement with those previously obtained in the *LiFh-cipro-in* system and by DFT calculations. The intense peaks observed for the Li^+-O's of the drug suggest a strong interactions, especially with the O1, one of the oxygens of the carboxylic group. The Li^+ are closer to the *O* of the drug than to the *O* of the clay. However, due to the orientations of the molecules and the confinement effect in the interlayer space, the *F* atoms of the cipro molecules are more hindered to interact with the Li^+ that is why the intensity of the signal is lower.

The radial distribution function of the Hydrogens of the amine group (H1) with the oxygens of the clay and with the oxygens and fluorine of the neighbor drugs are presented in Fig. 9. The analysis of this rdf gives information about the possible intermolecular hydrogen bonds, the involved atoms and the distances of these interactions. The O_2 atoms (the second oxygen of the carboxylic group) and the O_3 atoms (ketone oxygen) are the oxygens of the drug that are closest to the H1 atoms of the next molecule. These distances and their intensities suggest that strong H-bonds interactions are established in the system. Also, the O1 atoms can interact with the H1 atoms at distances associated with H-bonds, but they have a wider signal, suggesting longer interval of dH1-O1 in the system. It is important to remark, that the O1 atoms are mainly interacting with the Li^+ cations of the clay. The signals of the H1-Oclay and H1-F pairs appear at bigger distances and are less intense, suggesting that these interactions are not favored.

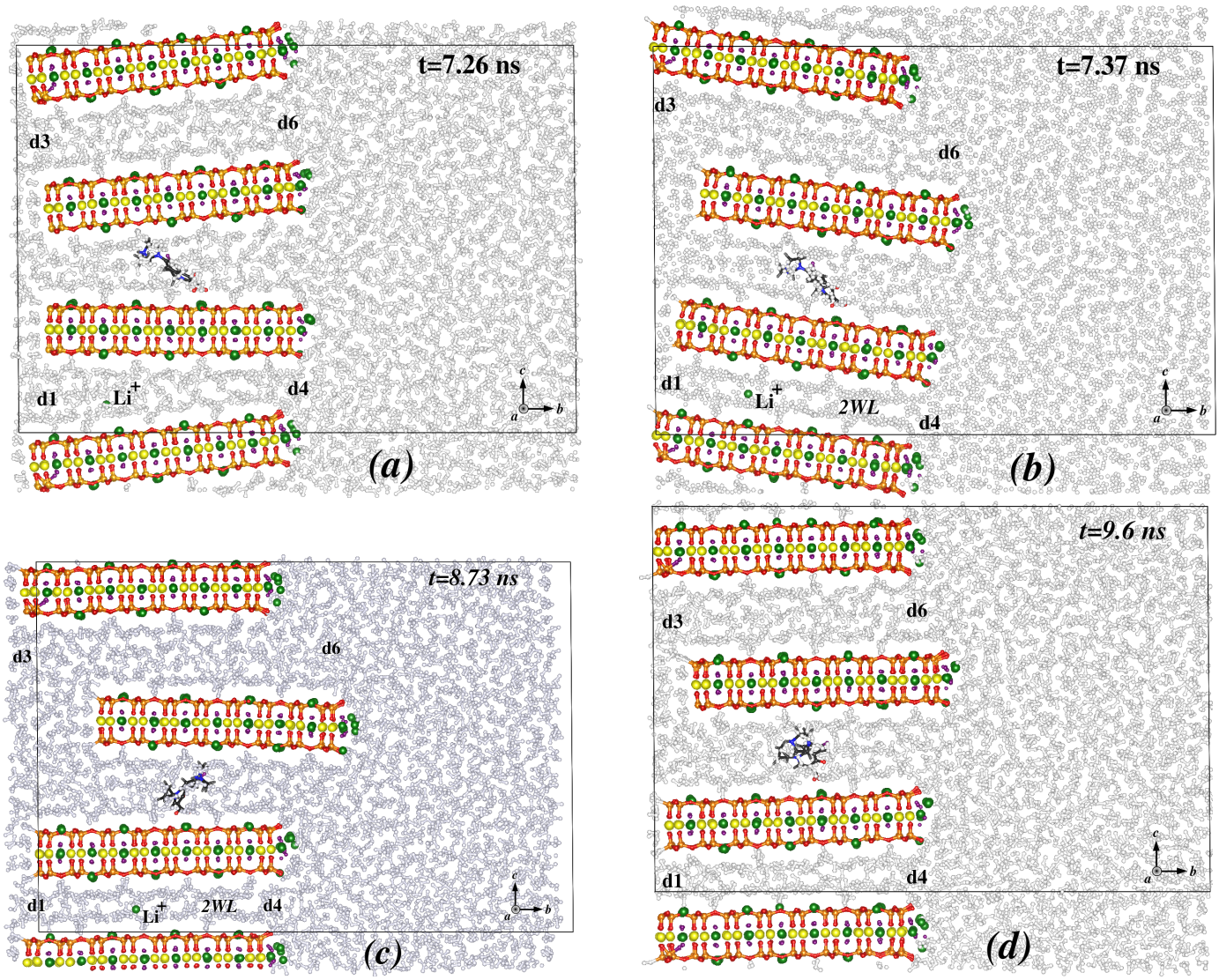

Figure 6. Different snapshots of the *LiFh-cipro-in* simulation. Orange, red, green, yellow, violet, black, white, and blue balls correspond to *Si*, *O*, *Li*, *Mg*, *F*, *C*, *H* and *N* atoms, respectively.

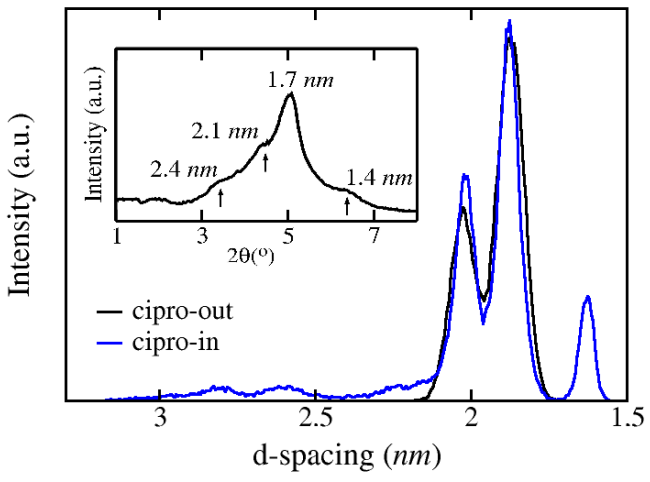

Figure 7. Histogram of the d-spacings of the *LiFh-cipro-out* (black line) and *LiFh-cipro-in* (blue line). In the inset the DRX pattern of *LiFh*-cipro [5] is shown.

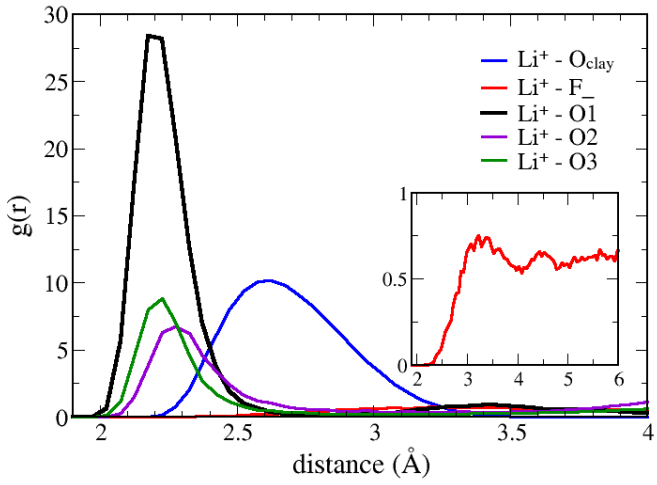

Figure 8. Radial distribution function of the Li^+ and the oxygens of the clay and the oxygens and fluorine of the cipro molecules.

Figure SI8 of the Supporting information shows the radial distribution function of the hydrogen atoms of the cipro molecule (H) with the oxygens of the clay and with the oxygens and fluorine of the neighbor drugs. Due to the geometry of the cipro molecule, this rdf includes information about the intramolecular interactions. Specifically, the first peaks of the H-F and $H-O3$ signals are associated with this kind of interaction. On the other hand, O1 and $O2$ atoms interact with H atoms at distances bigger that the recorded for Li^+ cations and H1 atoms.

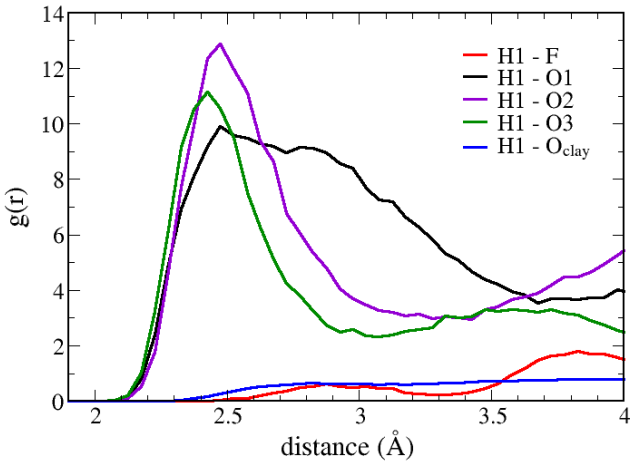

Figure 9. Radial distribution function of the Hydrogens of the amine groups and the oxygens of the clay and the oxygens and fluorine of the cipro molecules.

Finally, Fig. 10 shows some of the possible interactions that could be found if a high amount of cipro molecules are incorporated into the interlayers of the *LiFh* clay. These are the interactions resulting three neighbors molecules confined at the same interlayer at the end of the simulation.

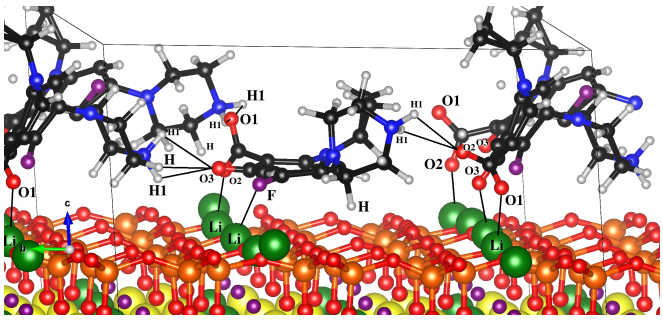

Figure 10. Interactions present in the *LiFh-6cipro* system at the end of the simulation. Only three neighbor molecules in the same interlayer are shown. The others three molecules are hidden to improve the visualization. Orange, red, green, yellow, violet, black, white, and blue balls correspond to *Si*, *O*, *Li*, *Mg*, *F*, *C*, *H* and *N* atoms, respectively. In the Figure, two cipro molecules appears twice considering periodic boundary conditions.

IV. CONCLUSIONS

A useful combination of theoretical calculations has been used in order to shed lights on the nature of the *LiFh*-cipro interactions. First principle and Molecular Dynamics calculations suggest that important electrostatic interactions are present when the cipro molecules are inside the *LiFh* framework. These are established mainly by the Li^+ cations of the clay, and the oxygen and fluorine atoms of the cipro molecule. Moreover, due to the confinement effect of the guest molecules, a high number of intermolecular and intramolecular hydrogen bonds between the drug molecules are observed inside the clay interlayer. These facts contribute to the stabilization of the drug. Dispersion contributions play an important role and should be taken into account in this kind of system. Their inclusion decreases the d-spacing, emerging and reinforcing the H-bonds and electrostatic interactions and permitting important energy stabilization.

Molecular dynamics calculations show a rapid migration of the Li^+ compensating cations located near the surface of the octahedral sheets, suggesting a charge reorganization process. Even when it is not possible to observe the full incorporation of the cipro inside the interlayer space due to the short scale of simulation time compared with the experimental one at least two attempts were identified. The simulation also shows different kinds of interactions between the drug and the clay in the first stages. Three water layers were located in the interlayer spaces of the *LiFh-cipro-out* system. And even when a solution with a high content of water was put in contact with the clay no signal of the swelling process was observed. However, once the drug is intercalated in the clay interlayer (*LiFh-cipro-in* system), the interaction of the outer water produces the displacement of the clay layers, suggesting that first stage of the swelling process is taking place. Also, the diffusion of one Li^+ compensating cation through the interlayer region and in the external solution is observed. The histogram obtained from the analysis of the d-spacings during the simulations of the *LiFh-cipro-out* and *LiFh-cipro-in* sheds lights on the possible conformations and arrangements of the cipro molecule and the water molecules in the clay interlayer and is in good agreement with the DRX pattern of the *LiFh*-cipro [5]. In the composite *LiFh*-cipro, the drug molecule is well anchored, and any indication of drug desorption process was not observed.

ACKNOWLEDGEMENTS

A.L. would like to honor and validate Professor Zicovich-Wilson's invaluable contribution to this paper. Sadly, Dr. Zicovich-Wilson passed away during the preparation of the manuscript. A.L. thank Mexican CONACyT for funding through project CB-178853 and SECITI-CLAF 2014 research scholarship. Thanks are due to DGTIC, UNAM for generous allocation of supercomputing time under grants SC16-1-IG-82 and LANCAD-UNAM-DGTIC-010 on Miztli supercomputer. Professor J. O. Fossum is acknowledged for facilitating the inclusion of our work in the Scientific Research Abstracts of 16 IZCC. Professor E. Altshuler and M. Lam are thanked for the revision of the manuscript. The authors also thank the University of Havana and the 16 IZCC organizing committee for financial support.

SUPPORTING INFORMATION

Supporting Information includes the Figures and the Table cited in the manuscript, the detailed information of the potentials and parameters used in the simulations, and the final geometries of all simulations reported in the manuscript.

Further videos related to the article can be found at:

- Video of the *LiFh-cipro-out*: https:www.youtube.com/watch?v=Kic_Fvpl3S4
- Video of *LiFh*_cipro_in: https://youtu.be/UjbVv6Z1C4c
- Video of *LiFh*_cipro_in_zoom, to see the interaction drug-clay: https://youtu.be/ENd3cU9R9uw
- Video of *Li* diffusion in: https://youtu.be/2IL3ib4stm8

BIBLIOGRAPHY

[1] M. Hanif, F. Jabbar, S. Sharif, G. Abbas, A. Farooq, and M. Aziz, Clay Miner. **51**, 469 (2016).

[2] I. Calabrese, G. Cavallaro, C. Scialabba, M. Licciardi, M. Merli, L. Sciascia, and M. Liveri, Int. J. of Pharm. **457**, 224 (2013).

[3] A. Hamilton, G. Hutcheon, M. Roberts, and E. Gaskell, Appl. Clay Sci. **87**, 129 (2013).

[4] D. Hernández, L. Lazo, L. Valdes, L. C. Ménorval, Z. Rozynek, and A. Rivera, Appl. Clay Sci. **161**, 395 (2018).

[5] A. Rivera et al., Appl. Clay Sci. **124-125**, 150 (2016).

[6] L. Valdés, D. Hernández, L. De Ménorval, I. Pérez, E. Altshuler, J. Fossum, and A. Rivera, Eur. Phys. J. Spec. Top. **225**, 767 (2016).

[7] L. Valdés, S. A. Martín, D. Hernández, L. Lazo, L. C. Ménorval, and A. Rivera, Rev. Cubana Fis. **34**, 35 (2017).

[8] L. Valdés, I. Pérez, L. Ménorval, E. Altshuler, J. Fossum, and A. Rivera, PLoS One **12**, e0187879 (2017).

[9] P. D. Kaviratna, T. J. Pinnavaia, and P. A. Schroeder, J. Phys. Chem. Solids **57**, 1897 (1996).

[10] E. C. dos Santos et al., RSC Adv. **7**, 26537 (2017).

[11] A. Seppälä, E. Puhakka, and M. Olin, Clay Miner. **51**, 197 (2016).

[12] J. Suter, R. Anderson, C. Greenwell, and P. Coveney, J. Mater. Chem. **19**, 2482 (2009).

[13] T. V. Shapley, M. Molinari, R. Zhu, and S. C. Parker, J. Phys. Chem. C **117**, 24975 (2013).

[14] J. L. Suter, D. Groen, and P. V. Coveney, Adv. Mater. **27**, 966 (2015).

[15] J. Breu, W. Seidl, and J. Senker, Z. Anorg. Allg. Chem. **630**, 80 (2004).

[16] T. J. Tambach, P. G. Bolhuis, E. J. M. Hensen, and B. Smit, Langmuir **22**, 1223 (2006).

[17] R. Dovesi et al., Int. J. Quantum Chem. **114**, 1287 (2014).

[18] I. Turel and G. Amalija, Anal. Sci. **19**, 329 (2003).

[19] C. Adamo and V. Barone, J. Chem. Phys. **110**, 6158 (1999).

[20] K. Valdiviés-Cruz, A. Lam, and C. M. Zicovich-Wilson, J. Phys. Chem. A **118**, 5779 (2014).

[21] K. Valdiviés-Cruz, A. Lam, and C. Zicovich-Wilson, J. Phys. Chem. C **121**, 2652 (2017).

[22] K. Valdiviés-Cruz, A. Lam, and C. M. Zicovich-Wilson, Phys. Chem. Chem. Phys. **17**, 23657 (2015).

[23] H. J. Monkhorst and J. D. Pack, Phys. Rev. B **13**, 5188 (1976).

[24] R. Dovesi et al., CRYSTAL 14 User's Manual edited by Univ. of Turin, Turin, Italy, (2014).

[25] S. Grimme, J. Comput. Chem. **27**, 1787 (2006).

[26] H. Berendsen, J. P. M. Postma, W. van Gunsteren, and J. Hermans, Interaction models for water in relation to protein hydration. In Intermolecular Forces, (Pullman, B., Ed.; D. Reidel: Amsterdam, 1981) pp. 331.

[27] M. Pouvreau, J. A. Greathouse, R. T. Cygan, and A. G. Kalinichev, J. Phys. Chem. C **121**, 14757 (2017).

[28] I. Todorov, W. Smith, K. Trachenko, and M. Dove, J. Mater. Chem. **16**, 1911 (2006).

[29] R. T. Cygan, J.-J. Liang, and A. G. Kalinichev, J. Phys. Chem. B **108**, 1255 (2004).

[30] V. Marry, E. Dubois, N. Malikova, S. Durand-Vidal, S. Longeville, and J. Breu, Environ. Sci. Technol. **45**, 2850 (2011).

[31] S. Koneshan, J. C. Rasaiah, R. M. Lynden-Bell, and S. H. Lee, J. Phys. Chem. B **102**, 4193 (1998).

[32] A. K. Rappe, C. J. Casewit, K. S. Colwell, W. A. Goddard, and W. M. Skiff, J. Am. Chem. Soc. **114**, 10024 (1992).

[33] L. Aristilde and G. Sposito, Environ. Toxicol. Chem. **27**, 2304 (2008).

[34] L. Aristilde and G. Sposito, Environ. Toxicol. Chem. **29**, 90 (2010).

[35] I. Turel, P. Živec, A. Pevec, S. Tempelaar, and G. Psomas, Eur. J. Inorg. Chem. **2008**, 3718 (2008).

[36] O. Cramariuc, T. Rog, M. Javanainen, L. Monticelli, A. V. Polishchuk, and I. Vattulainen, Biochim. Biophys. Acta, Biomembr. **1818**, 2563 (2012).

[37] R. Toth, A. Coslanich, M. Ferrone, M. Fermeglia, S. Pricl, S. Miertus, and E. Chiellini, Polymer **45**, 8075 (2004).

[38] D. W. Scott, Biometrika **66**, 605 (1979).

[39] D. W. Scott, Wiley Interdisciplinary Rev. Comput. Stat. **2**, 497 (2010).

[40] P. Mignon, P. Ugliengo, M. Sodupe, and E. Hernandez, Phys. Chem. Chem. Phys. **12**, 688 (2010).

[41] F. Salles, *et. al*, J. Phys. Chem. C **112**, 14001 (2008).

[42] F. Salles, *et. al*, J. Phys. Chem. C **119**, 10370 (2015).